

Smart window based on integration of nanoporous microparticles in liquid crystal composite with metamaterial nanostructured VO₂ film

Sofiia Barinova^{a,*}, Saranya Bhupathi^{b,c}, Peter G. Kazansky^d, Yi Long^{b,c}
and Ibrahim Abdulhalim^{a,c,*}

^aBen-Gurion University of the Negev, School of Electrical and Computer Engineering, Ilse-Kats Center for Nanoscale Science and Technology, Department of Electro-optics and Photonics Engineering, Beer Sheva, Israel

^bNanyang Technological University, School of Materials Science and Engineering, Singapore

^cSingapore-HUJ Alliance for Research and Enterprise, Nanomaterials for Energy and Energy-Water Nexus, Campus for Research Excellence and Technological Enterprise, Singapore

^dUniversity of Southampton, Optoelectronics Research Centre, Southampton, United Kingdom

ABSTRACT. Smart window devices have garnered significant attention recently. Traditional thermochromic windows can control infrared (IR) radiation but not visible light, whereas liquid crystals (LCs) control visibility through voltage-controlled scattering, neglecting IR control due to forward scattering. We demonstrate that nematic LCs with a minor concentration of nanoporous microparticles (NMPs) can rapidly modulate transparency in thin devices called NMP-LCs. To concurrently control both visible and IR spectra, we propose combining a layer of ultrashort pulsed laser-patterned vanadium dioxide (VO₂) with a 2% NMP composite in the LC. The patterned VO₂ film serves two key functions: (i) inducing LC alignment along the nanograting lines formed by pulsed laser patterning and (ii) enabling IR radiation control with enhanced thermochromic properties compared with closed structures. The LC component facilitates visibility control via voltage or temperature modulation. The combined system thus presents a superior smart window solution, capable of efficiently managing heat and visibility with high-speed response, low voltage requirements, and minimal LC and NMP concentrations.

© 2024 Society of Photo-Optical Instrumentation Engineers (SPIE) [DOI: [10.1117/1.JPE.14.048001](https://doi.org/10.1117/1.JPE.14.048001)]

Keywords: liquid crystal devices; VO₂; hybrid smart windows

Paper 24037G received Jun. 27, 2024; revised Sep. 3, 2024; accepted Sep. 17, 2024; published Oct. 10, 2024.

1 Introduction

Due to the rapid growth in population and technological advancement, modern society consumes an enormous amount of energy. In ancient times, energy consumption was minimal, around 3 kWh per day per person, primarily for food. Today, the global average primary energy consumption stands at 58 kWh per day per person, with countries such as the United States and Germany, recording much higher figures of 219 and 120 kWh per day, respectively.¹

A significant portion of a building's energy consumption, ~40%, is attributed to heating, ventilation, and air conditioning systems.² This substantial energy consumption contributes to environmental pollution and resource depletion. Thus, the implementation of energy-saving

*Address all correspondence to Sofiia Barinova, sofiab@post.bgu.ac.il; Ibrahim Abdulhalim, abdulhlm@bgu.ac.il

strategies, such as using smart windows for temperature control, has become increasingly important.

The amount of heat that comes from the sun into a room through a standard window depends on several factors, such as the size and orientation of the window, the type of glass, the angle of sunlight, the time of the day, and the season. However, we can estimate the heat gain based on some general assumptions. Factors affecting solar heat gain include: (i) solar irradiance: the average solar irradiance on the earth's surface is $\sim 1000 \text{ W/m}^2$ on a clear day when the sun is directly overhead; (ii) window area: the size of the window affects how much sunlight enters the room; (iii) window glass properties: the type of glass (e.g., single-pane, double-pane, and low-E coating) impacts how much solar radiation is transmitted, absorbed, or reflected; (iv) angle of incidence: the angle at which sunlight hits the window determines how much of the solar energy is absorbed or reflected, and (v) shading devices: blinds, curtains, and other shading devices can reduce the amount of solar heat entering the room. Here is a simplified estimation: with the solar heat gain for a standard window under ideal conditions (clear day, direct sunlight) assuming a typical window size of 1.5 by 1.5 m (area of 2.25 m^2) and assuming solar irradiance of 800 W/m^2 accounting for the average conditions when the sun is not directly overhead, a glass transmission for a standard clear single-pane window, $\sim 80\%$ of solar energy may be transmitted. We get heat gain calculated as follows: heat gain = solar irradiance \times window area \times transmission factor = $800 \text{ W/m}^2 \times 2.25 \text{ m}^2 \times 0.80 \approx 1440 \text{ W}$, entering the room through a standard window under these conditions. To remove this heat, a full-capacity air conditioner is required. The operating power of the window can be reduced further; see, for example, the normally bright mode of the smart window we demonstrated recently.³ Other possibilities for reducing operating energy are the use of liquid crystal (LC) bistable mode, which are working on.

Various technologies can be used for temperature and visibility control, such as hydrogels,⁴ ionic liquids,⁵ metamaterials,^{6,7} and perovskites.⁸ Smart thermochromic windows offer temperature regulation, complementing traditional heating and cooling systems. However, they do not address visibility control in the visible range. Hydrogels have several advantages: inexpensive, easy to process, and biocompatible; they offer a passive, energy-free mechanism for temperature and visibility control. Their limitations are: the response time can be slow, and they may suffer from mechanical degradation over time; they may not provide as precise control over light transmission as some other technologies. The advantages of ionic liquids include high thermal stability, can be tuned to achieve specific optical properties, and enable active control over visibility with low power consumption. They have several limitations: they need external power for operation, making them less energy-efficient than passive materials, and there are potential issues related to long-term stability and cost. The advantages of metamaterials include precise control over both temperature and visibility; they can be designed to respond to a wide range of stimuli; and they can achieve effects that are difficult or impossible with conventional materials, such as negative refractive indices or perfect absorption. Their limitations include the complexity of manufacturing at a large scale, which is a significant barrier, and they can be expensive and challenging to integrate into existing window technologies. Perovskites have several advantages: they offer high tunability and efficiency, with the potential for integration into photovoltaic devices for energy generation; they can be fabricated using low-cost solution processes. Their limitations include stability as a major issue for perovskites, particularly under prolonged exposure to light and moisture; the technology is still relatively new, and long-term performance data is limited. Smart thermochromic windows offer temperature regulation, complementing traditional heating and cooling systems. However, they do not address visibility control in the visible range.

However, LC windows control visibility through scattering, but they scatter both visible and infrared (IR) light in the forward direction, as the scattering is of Mie type, allowing all radiation to enter the building, thereby failing to control the temperature effectively. To address this limitation, we recently introduced a hybrid window,⁶ which combines the VO_2 film with an LC tunable scattering window based on Cochleates organic particles in an LC composite. This innovative approach enables simultaneous control of temperature and visibility, enhancing comfort and energy efficiency. In addition, in a related study,⁷ we explored a similar concept using VO_2 nanoporous microparticles (NMPs) instead of cochleate organic particles, further demonstrating the versatility and effectiveness of this approach in smart window technology. The composite

NMP-LC was developed in our group using a variety of NMP types: nanoporous Si,⁹ cigar-shaped cochleate particles,^{3,10} colloids of decanol,¹¹ and VO₂ NMPs.⁷ NMPs have two roles; the first is that when the LC penetrates the nanopores, it reduces the effective index of the NMP to become closer to one of the indices of the LC (n) so that a large (small) index mismatch exists at zero voltage when the alignment is homogenous^{7,9-11} (when the alignment is homeotropic³), hence the scattering state (transparent state), and a small (large) index mismatch at high voltage so it becomes transparent (scattering). The two modes of normally scattering^{7,9-11} or normally bright³ windows were demonstrated by us. The second role is to make its density closer to that of the surrounding LC, so it does not precipitate or float. We should also mention that the particles are hydrophobic, meaning that the LC molecules are arranged perpendicular to their surface.

To improve the thermochromic properties of VO₂, different approaches were proposed, such as the bioinspired solution for spectrally selective thermochromic VO₂,¹² Moth eye structure,¹³ crystals structures,¹⁴ and smart window coating using a stoichiometrically downgraded vanadium oxide.¹⁵ Other smart window approaches include the use of hydrogel,^{16,17} ionic liquids,^{18,19} the application of thermo-responsive metamaterials to energy-efficient smart window applications, perovskites,²⁰ and LCs.^{6,7,21}

In this study, a patterned VO₂ thin film was utilized due to its improved thermochromic properties, particularly due to a reduction in Fresnel reflection. Subwavelength structures on the surface of optical interfaces have been known as an effective method of reducing Fresnel reflections, creating an effective refractive index gradient between the air and the medium. The use of patterned thin films offers several advantages, including enhanced control over the optical properties of the material. This approach not only reduces unwanted reflection losses but also enhances the device's ability to modulate IR radiation and optimize its thermal properties. The reader is referred to our detailed study of femtosecond (fsec) laser-patterned VO₂ film thermochromic properties published in our earlier paper.²²

In this study, we integrated a patterned VO₂ layer with a composite LC smart window. Although VO₂ alone can control IR radiation, it does not affect visibility in the visible spectrum. However, the LC layer controls visibility but does not effectively manage total IR energy due to forward scattering. The hybrid window design allows for simultaneous control of heat and transparency using temperature and voltage. The concept is illustrated in Fig. 1. Panels (a) and (b) demonstrate the LC window's ability to control forward scattering of both visible and IR light in summer and winter. Panels (c) and (d) show the behavior of the VO₂ window alone, reflecting IR in summer and allowing transmission in winter. Panels (e) and (f) showcase the hybrid window's capabilities, reflecting IR in summer and transmitting IR in winter while controlling visibility in the visible spectrum through controlled scattering by the LC in both seasons.

To describe the behavior of the LC layer, let us consider Figs. 1(a) and 1(b): this structure can allow IR radiation to pass through without control while controlling the passage of visible light. It can function like a curtain, altering visibility depending on a small amount of applied voltage. As shown in Fig. 1(a), all radiation (except for small reflections) is scattered, making the glass opaque, indicating a mode with reduced visibility. In contrast, Fig. 1(b) shows the glass as completely transparent, allowing both types of radiation to pass through (except for small reflections), resulting in a transparent mode.

To describe the VO₂ layer's behavior, refer to panels (c) and (d). In the summer mode [Fig. 1(c)], visible light passes through with minimal reflection, whereas IR radiation is mostly reflected. In the winter mode [Fig. 1(d)], both visible and IR radiation pass through with minimal reflections. For the hybrid cell, see panels (e) and (f). The LC and VO₂ layers each control one type of radiation: LC for visible light and VO₂ for IR. Combining these materials allows the hybrid structure to control both types of radiation.

Using the fsec laser patterning, we obtained recently better results than a closed film of VO₂.¹⁸ Therefore, this hybrid window is expected to have the potential for energy saving and privacy control. The nano-patterned surface also aligns the LC molecules along the nano grooves created by the ultrafast-pulsed laser; thus, there is no need for an additional aligning layer on the VO₂ surface. This fact was proved by our group on fsec laser-patterned indium tin oxide (ITO).^{3,10}

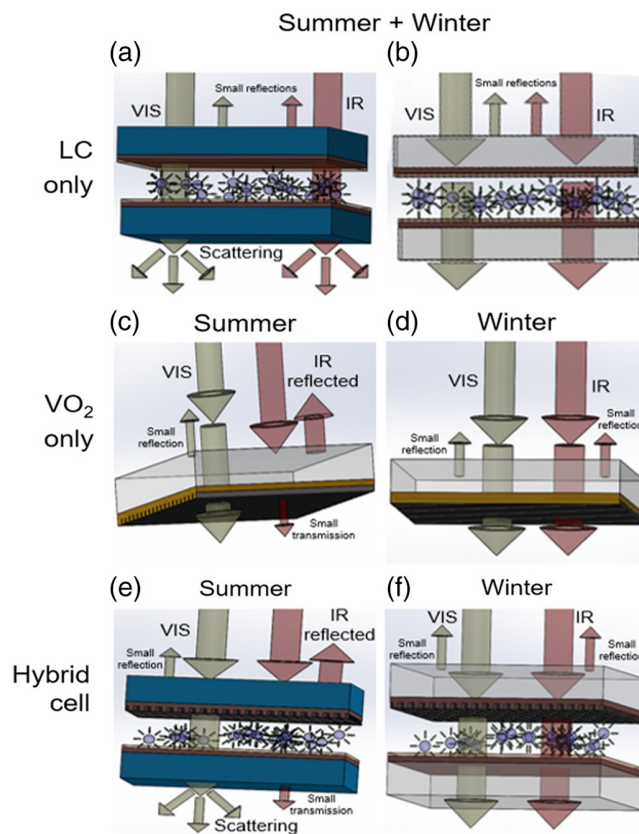


Fig. 1 (a) Only LC, $V = 0 \geq$ less visibility, (b) only LC, $V > 0 \geq$ controlled visibility, (c) only VO_2 , reflection IR mode for summer, (d) only VO_2 , transmission IR mode for winter, and (e) and (f) hybrid cell, unites properties LC and VO_2 : transmit or reflect IR and controlled visibility.

2 Experimental Part

The substrate (BL7 glass) was cleaned by midfrequency (MF) sputter-etching for 1800 s using 300 sccm of argon gas at a constant pressure of 250 mPa at 650 V with a frequency of 240 kHz, 1600 ns on time. After that, VO_2 thin film was deposited using physical vapor deposition (PVD, Cemecon CC800/9 ML PVD system, Würselen, Germany). The vanadium source is a 390 cm^2 99.9% purity vanadium target provided by Cemecon. To produce pattern four (Fig. 2), a femto-second laser system PHAROS (Light Conversion Ltd., Suwalki, Poland) operating at a wavelength of 1030 nm with a pulse duration of 180 fs and repetition rate of 500 kHz was used. Optimization work was done to create the best surface, and for that, the reader is referred to Ref. 12. Here, we present only the scanning electron microscope and the atomic force microscope images of the optimum pattern shown in Fig. 2.

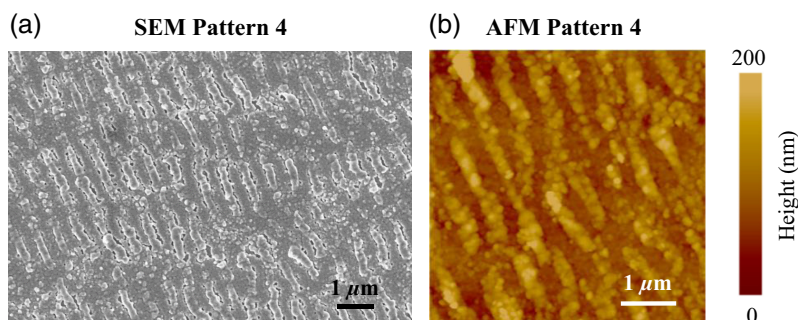


Fig. 2 (a) SEM and (b) AFM images of the femto-second laser-structured VO_2 thin-film surface with pattern four. The area of this pattern is $\approx 3 \text{ mm} \times 3 \text{ mm}$. The pulse number is 50, and its energy is 7 nJ.²²

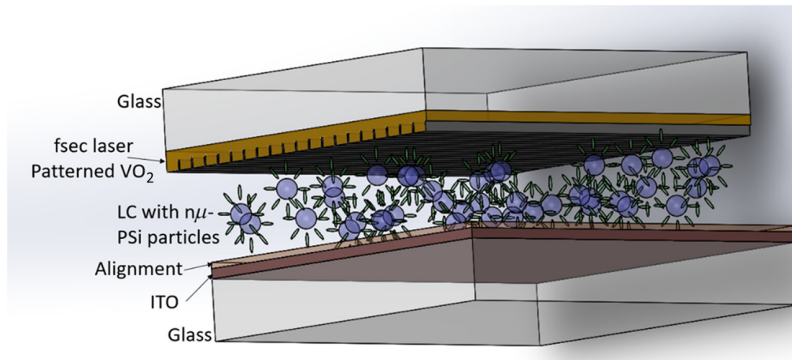


Fig. 3 Cell structure.

The second substrate is made of glass coated with an ITO transparent electrode prepared in several steps. First step: ultrasonic cleaning with distillate water, acetone, and isopropanol; checking substrate under the microscope and cleaning it by hand with acetone. Second step: spin coating of the clean substrate with SE410 Nissan polyimide and bake it in the oven: start from 90°C, reach 180°C, and wait for 2 h. Afterward, reduce the oven temperature to room temperature and leave the substrates inside until they cool to room temperature. Third step: rubbing substrate using velvet cloth in one direction.

This device needed an LC layer thickness of 13 microns, and to produce it, we used mylar sheets. The mylar was glued with optical UV paste irradiated for 10 min under a UV lamp. Then, the prepared cell is filled with a mixture of 2 wt% pSi particles in LC BL036. Next step, the cell was closed up by the VO₂ side and then sealed from all sides with UV paste. Finally, electrical contacts have been added with silver paste and UV glue. The cell structure is shown in Fig. 3.

The cell was examined under a microscope (Fig. 4) at 5× magnification in transmission mode between crossed polarizers. The first row [panels (a)–(c)] represents images taken without the application of voltage, whereas the second row [panels (d)–(f)] shows images captured under 60 V. A comparison can be made between pairs: (a) with (d), (b) with (e), and (c) with (f), illustrating the voltage dependence. The first and second columns are oriented at 0 and 45 deg, respectively, with respect to the polarizers. The third column shows the image without the polarizer.

Figure 5 shows images taken through the device with and without voltage. In Figs. 5(a) and 5(b), images through the device are shown at 0 and 90 V, respectively. In Fig. 5(a), which

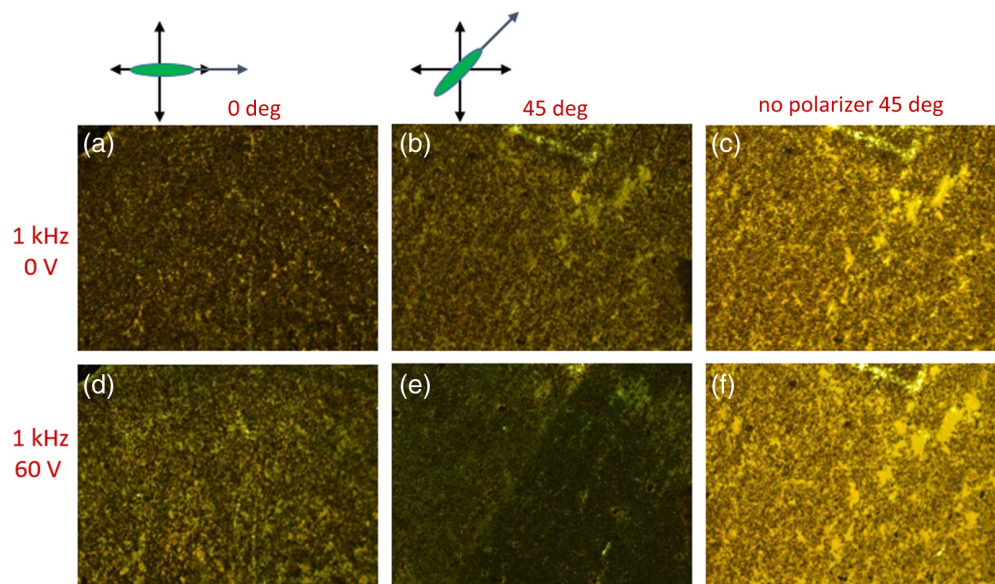


Fig. 4 Polarizing optical microscopy images.

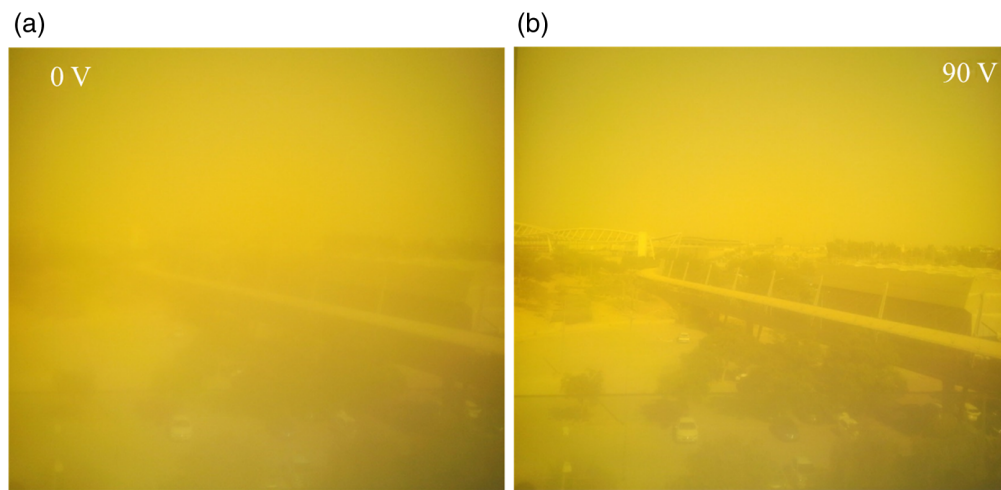


Fig. 5 Photos through the cell in the opaque and transparent states at room temperature.

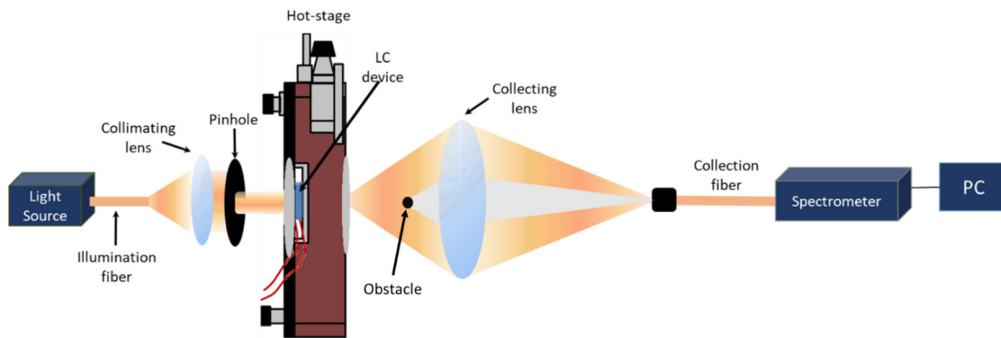


Fig. 6 Schematic of the experimental setup used for the scattering measurements.

represents the device in a less transparent state at 0 V, visibility is significantly reduced. Conversely, in Fig. 5(b), depicting the device in a more transparent state at 90 V, visibility is improved, offering a clearer view. This demonstration highlights the device's ability to modulate transparency based on the applied voltage.

We present photographs taken through the cell only at room temperature because the transition temperature for the LC is just above 90°C, and it is difficult to carry the device with the heating stage and setup to the building window for pictures.

The measurement setup for the scattering is shown in Fig. 6. The light from the fiber-coupled light source is collimated and passes through a pinhole with a 1-mm diameter. To measure the scattered light, an obstacle is added near the center of the collection lens to stop the non-scattered light from arriving at the output fiber, which is connected to the spectrometer at its distal end.

To calculate relative scattering, we divide the scattering value obtained with the setup that includes the obstacle (as shown in Fig. 6) by the scattering value measured without the obstacle. LC device in Fig. 6 is the one from Fig. 3.

Devices and equipment used: Light source for the visible range VIS—StellarNet Inc. SL S/ N: 12040906, Tampa, Florida, United States; Light source for the IR range—ThorLabs SLS 202, Newton, New Jersey, United States; Spectrometer VIS—Ocean Optics; Spectrometer IR—StellarNet Inc. DS-InGaAs-512 NIR-25 BW Spectrometer.

3 Results and Discussion

The results for scattering in visible light at room temperature [Figs. 7(a)] are exhibiting interesting behavior. Plots for different voltages cross at 700 nm wavelength. Behavior in IR expected scattering increases with decreasing voltage. The sudden increase of scattering for $\lambda < 700$ nm can be due to aggregated particles at 0 V, which start to separate as voltage is applied, thus

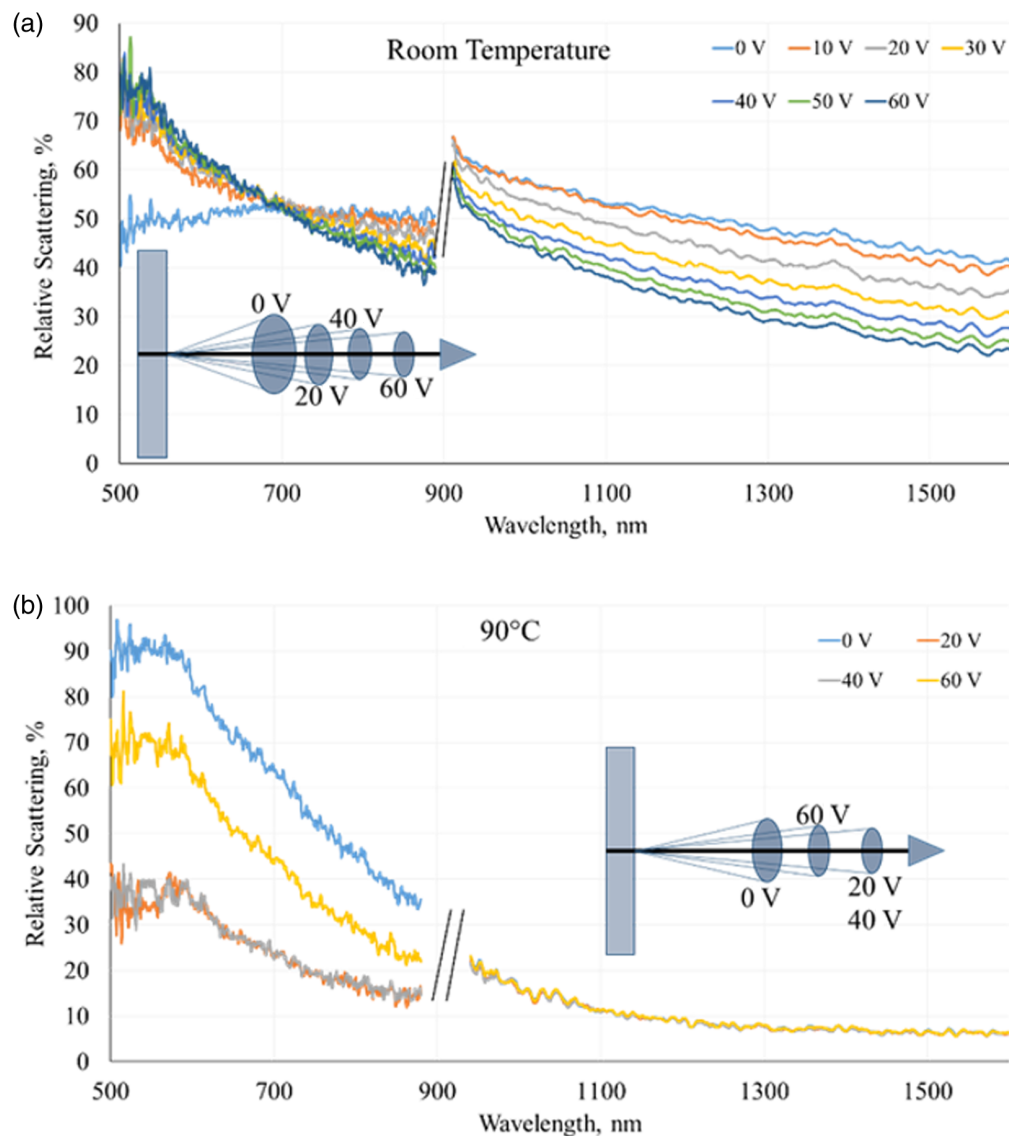


Fig. 7 Scattering measurements in VIS and IR at room temperature (a) and at 90°C (b). Please note that measurements near 900 nm are not continuous. This is because two spectrometers were used: one covering the visible (VIS) range up to 900 nm, and another covering the IR range starting from 900 nm. The transition between these spectrometers occurs ~900 nm, where both instruments exhibit higher noise levels, leading to relatively large errors in this region. Consequently, due to the noise in this overlapping area, we have presented the data in segments rather than continuously.

making the particle-LC domain comparable to the wavelength. This also explains the larger scattering in the IR range at 0 V.

Figure 7(b) shows behavior above transition temperature. In the VIS range, there exists voltage dependence but not in the IR range. Most likely, this is due to the same aggregation phenomenon that is eliminated at high temperatures, thus making the particle-LC domain much less than the wavelengths in the IR but comparable to those in the visible range.

The difference in the behavior between Figs. 7(a) and 7(b) is illustrated schematically with the scattering cone size shown on each figure. Figure 7(a) demonstrates for room temperature larger scattering for 0 V—larger cone and less scattering for 60 V.

Figure 8 shows total transmission (TT). For TT measurements, a setup that includes an integration sphere was used as described elsewhere.⁷ For RT in VIS, the minimum is around 40% but for IR, ~80%. For transition temperature, TT drops significantly. Around transition temperature,

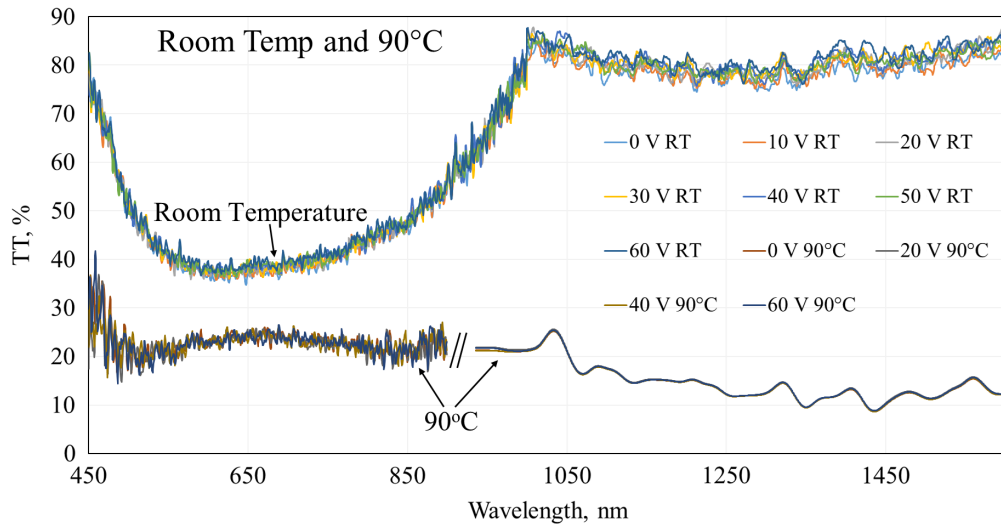


Fig. 8 TT for VIS and IR at room temperature and 90°C.

this device has a lot of scattering. The more it is heated, the more the scattering; as expected, the device deteriorated with time. Transmission of IR radiation is minimal at higher temperatures [Fig. 1(e)] as, in the metallic phase, the VO₂ reflects and absorbs the IR.

The fall and rise times shown in Fig. 9 illustrate the relatively fast response of this device; in particular, the rise time is in the sub-msec range at high enough voltages. For room temperature and 85°C temperatures, the behavior of the rise time is expected as $\tau \propto 1/V^2$. However, the fall time decreases drastically with voltage, which is not the normal behavior as the relaxation time of nematic LCs is constant at least at low voltages. The reason is that this LC device is not an ideal pure nematic LC with perfect alignment as the particles produce domains. With uniform LC, the relaxation time originates from the backflow as the LC tries to relax back to the original state.

However, the backflow cannot exist with the NMPs inside. In addition, near the transition temperature to the isotropic phase, the temperature dependence of the elastic constants and the viscosity might be different in the NMP-LC system. More fundamental studies will be done in the future as, for smart window operation, the response time is not critical because it is already satisfying the requirements.

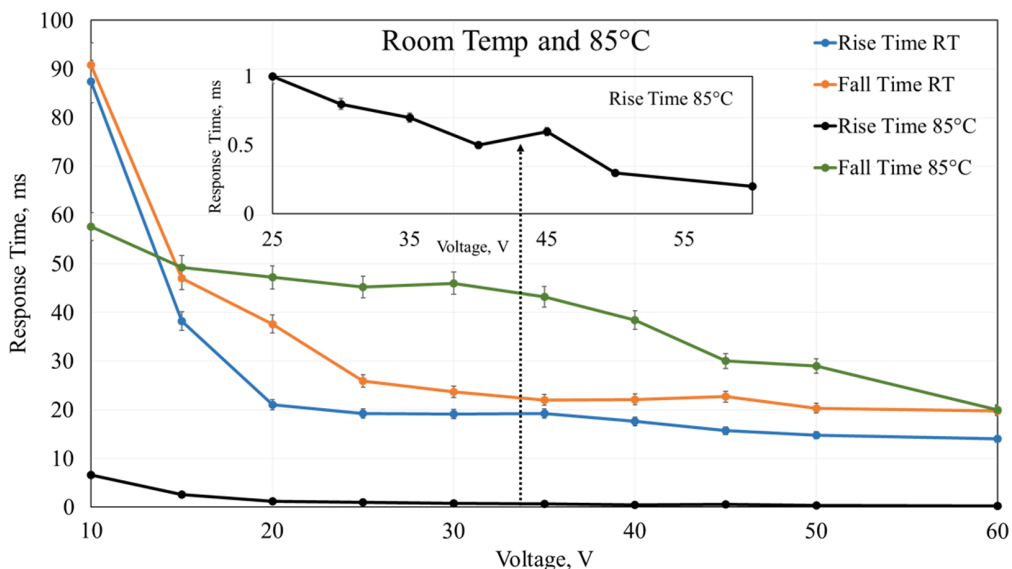


Fig. 9 Response times (rise and fall) versus voltage at room temperature and high temperatures. The inset shows the high voltage range at 85°C with higher resolution, showing that submsec response time is achieved.

4 Conclusion

The hybrid device, merging nanopatterned VO₂ with an LC composite (LC +2% NMPs), offers a range of advantages. By combining these materials, the device achieves dual control, effectively managing the visible and IR ranges. With voltage, the visibility is controlled due to the tunable scattering via the NMP-LC effect, whereas temperature controls the IR transmitted through the device because of the VO₂ thermochromic properties. This capability enhances energy efficiency and comfort in indoor environments.

Furthermore, the fsec laser nanostructured VO₂ exhibits superior thermochromic properties compared with conventional materials. This enhancement allows for more precise control over heat and light transmission, resulting in improved performance and comfort.

In addition, the nanograting produced by the fsec laser on the VO₂ surface facilitates the alignment of LC molecules. Overall, the hybrid device represents a significant advancement in smart window technology, offering a comprehensive solution for energy-efficient and comfortable indoor environments. Future developments are needed to bring it to a practically valuable smart window and include the reduction of the VO₂ insulator to metal transition; optimization of the operating power, for example, using the normally bright mode reported in ref.³ or bistable LC modes; and further optimization of the thermochromic properties of VO₂ by better design of the nanopattern.

Code and Data Availability

Data will be available upon request from the corresponding author.

Acknowledgments

The research is partially supported by the Israel Ministry of Energy and Infrastructure and by grants from the National Research Foundation, Prime Minister's Office, Singapore, under its Campus of Research Excellence and Technological Enterprise (CREATE) program.

References

1. J. Davenport and N. Wayth, "73rd statistical review of world energy," Energy Institute, p. 55 (2024).
2. M. Aburas et al., "Thermochromic smart window technologies for building application: a review," *Appl. Energy* **255**(1), 113522 (2019).
3. N. Huseen, Z. Judeh, and I. Abdulhalim, "Mesoporous cholesteric particles doped liquid crystal as normally transparent smart window," *Microporous Mesoporous Mater.* **379**, 113296 (2024).
4. G. Xu et al., "Thermochromic hydrogels with dynamic solar modulation and regulatable critical response temperature for energy-saving smart windows," *Adv. Funct. Mater.* **32**(5), 2109597 (2022).
5. Y. Pei et al., "Ionic liquids for advanced materials," *Mater. Today Nano* **17**, 100159 (2022).
6. P. Lakshmi Madhuri et al., "Hybrid vanadium dioxide-liquid crystal tunable non-reciprocal scattering metamaterial smart window for visible and infrared radiation control," *Opt. Mater. Express* **11**(9), 3023–3037 (2021).
7. S. Barinova et al., "Metamaterial hybrid smart window based on nanoporous VO₂ microparticles in liquid crystal for heat blocking and visibility control," *ACS Appl. Energy Mater.* **6**(14), 7587–7595 (2023).
8. Y. Zhang et al., "Perovskite thermochromic smart window: advanced optical properties and low transition temperature," *Appl. Energy* **254**, 113690 (2019).
9. P. L. Madhuri et al., "Voltage controlled scattering from porous silicon Mie-particles in liquid crystals," *J. Mol. Liq.* **281**, 108–116 (2019).
10. P. L. Madhuri et al., "Hybrid vanadium dioxide-liquid crystal tunable non-reciprocal scattering metamaterial smart window for visible and infrared radiation control," *Opt. Mater. Express* **11**(9), 3023–3037 (2021).
11. I. Abdulhalim et al., "Novel easy to fabricate liquid crystal composite with potential for electrically or thermally controlled transparency windows," *Opt. Express* **27**(12), 17387–17401 (2019).
12. A. Taylor et al., "A bioinspired solution for spectrally selective thermochromic VO₂ coated intelligent glazing," *Opt. Express* **21**(S5), A750–A764 (2013).
13. A. Taylor, "Motheys Smart Windows Bio-inspired, temperature-responsive glazing for passive regulation of building temperature with the ability to self-clean," Doctoral Thesis, University College, London (2017).
14. M. Feng et al., "Review: smart windows based on photonic crystals," *J. Mater. Sci.* **55**(35), 8444–8463 (2020).
15. M. K. Behera et al., "Potential low powered smart window coating using a stoichiometrically downgraded vanadium oxide thin film structure," *AIP Adv.* **10**(6), (2020).

16. Y. Zhou et al., "Liquid thermo-responsive smart window derived from hydrogel," *Joule* **4**(11), 2458–2474 (2020).
17. Y. Zhou et al., "Hydrogel smart windows," *J. Mater. Chem. A* **20**, 10007–10025 (2020).
18. R. P. Swatloski et al., "Dissolution of cellulose with ionic liquids," *J. Am. Chem. Soc.* **124**(18), 4974–4975 (2002).
19. Y. Ma et al., "Soft elastomers with ionic liquid-filled cavities as strain isolating substrates for wearable electronics," *Small* **13**(9), 1602954 (2016).
20. Y. Liu et al., "Full-frame and high-contrast smart windows from halide-exchanged perovskites," *Nat. Commun.* **12**, 3360 (2021).
21. S-W Oh et al., "A cholesteric liquid crystal smart window with a low operating voltage," *Dyes Pigm.* **197**, 109843 (2021).
22. S. Bhupathi et al., "Femtosecond laser-induced vanadium oxide metamaterial nanostructures and the study of optical response by experiments and numerical simulations," *ACS Appl. Mater. Interfaces* **12**(37), 41905–41918 (2020).

Biographies of the authors are not available.